IEEE Access
Multidisciplinary | Rapid Review | Open Access Journal

Received December 11, 2017, accepted February 24, 2018, date of publication March 9, 2018, date of current version April 18, 2018.

Digital Object Identifier 10.1109/ACCESS.2018.2814005

Investigation of Epidermal Loop Antennas for Biotelemetry IoT Applications

HAITHAM ABU DAMIS[1], (Student Member, IEEE), NABIL KHALID[1], (Student Member, IEEE), RASHID MIRZAVAND[1,2], (Senior Member, IEEE), HYUN-JOONG CHUNG[3], AND PEDRAM MOUSAVI[1], (Senior Member, IEEE)

[1]Intelligent Wireless Technology Laboratory, University of Alberta, Edmonton, AB T6G 2R3, Canada
[2]Electrical Engineering Department, Amirkabir University of Technology, Tehran 15914, Iran
[3]Department of Chemical and Materials Engineering, Faculty of Engineering, University of Alberta, Edmonton, AB T6G 2R3, Canada

Corresponding author: Nabil Khalid (nkhalid1@ualberta.ca)

This work was supported by NSERC-AITF Industrial Research Chair Program.

ABSTRACT The Quadruple Loop (QL) antenna was designed and investigated to deliver a robust body-worn antenna for bio-medical applications. The QL antenna is a very thin single-layer groundless structure which allows for the installation of neighboring electronics and sensors which need to be extremely close to the epidermis layer. The performance of the proposed antennas was investigated for three main standards: GSM-900, GSM-1800, and Bluetooth low energy (BLE). Radiation pattern measurements were conducted to compare their results with their simulation counterparts. Moreover, data communication tests showed that the acquired BER readings could qualify the BLE and GSM-900 antennas to work as part of 4-QAM wireless links. Besides these hands-on endeavors, an equivalent and more efficient mathematical model of biological tissues which make up the human arm was computed. The equivalent model was tested in software and has the practical potential to be realized in physical phantom making.

INDEX TERMS Epidermal antennas, wearable antennas, body-worn antennas, IoT, loop antennas, WBAN, WPAN.

I. INTRODUCTION

There is no doubt that the drive towards a ubiquitous presence of technology is desired to be both wirelessly and seamlessly connected to the internet. Hence, we are being increasingly exposed to the term "the Internet of Things" (IoT). This concept would soon be applied to numerous applications such as weather and traffic monitoring in addition to various other fields [1]–[4]. More importantly, the IoT is expected to serve the health care sector by providing outpatients with timely and reliable diagnostics through the use of wireless body sensors to screen and share biometrics with health-care professionals in real-time [5]. Such sensors should be functionally robust yet comfortable to wear. Due to many stringent and demanding requirements, novel body sensors are required to fulfill the expectations of future biotelemetry technologies.

Body-worn Antennas (BWA) is the umbrella term for all antennas placed in close proximity to an organism's body. This includes wearable, epidermal, and implanted antennas. Epidermal antennas [6], [7], as their name pertains, could be characterized by body-antenna separation gaps of less than 1mm. This gap is typically occupied by a dielectric substrate which is stretchable, flexible, adhesive, or a combination of all three features. If the antenna structure covers a substantial area of the skin, the substrate is expected to be breathable. Given these features, epidermal antennas are mostly applied in sensing and biomedical applications where body parameters such as skin-hydration levels and vital sign readings are to be transmitted wirelessly. Another challenge with all the BWAs is performance degradation due to their proximity to biological tissues. These tissues are characterized by high loss tangents and high relative permitivity. Such factors increase the design complexity of the body-worn antenna. Hence, the antenna type and substrate material must be carefully selected.

Several research groups started to contribute to this revolutionary field by developing different BWAs. However, their efforts were limited to the aspects of antenna design and operation in the lower frequency bands of RFID technology [6], [8]. Instead, more attention should be paid to the performance of BWAs as unconventional communication devices for other more popular frequency bands.

This is but one motivation for the work we present in this paper. Moreover, only a few articles have included measurements on actual human body volunteers. This is important since the radiation pattern for body-worn antennas measured on a human body provides more accurate and meaningful results than those taken from phantom measurements. In [9], the radiation pattern of a 1.5 GHz GPS antenna is shown which was measured on an actual human volunteer. An embroidered spiral antenna with its reflection coefficient was measured on a human abdomen [10], whereas the far-field radiation pattern was measured on a physical human phantom. A comparison of the simulated and measured far-field performance of a filtering antenna is reported in [11]. The scarcity of articles with measurements on a real human body can be attributed to the difficulty of standing moveless for prolonged measurements and the lack of access to large enough anechoic chambers.

This paper presents theoretical and experimental efforts undertaken in the investigation of three epidermal Quadruple Loop (QL) antennas. Each antenna was designed to operate in a specified frequency band: GSM-900, GSM-1800, and BLE. In addition, Error-vector magnitude (EVM) tests and BER metrics were conducted and calculated, respectively, to verify the integrity of GSM and BLE communications for the QL antennas.

The remainder of this article is organized as follows. Section II address the epidermal antenna topology and design. The simulations and modeling of antenna are presented in section III. Following that, section IV discusses the fabrication and performance tests of designed antennas and section V presents the data communication evaluations. Finally, the paper is concluded in section VI.

II. ANTENNA TOPOLOGY

BWA could be categorized into two main topology categories: mono-layer and multi-layer antennas. A mono-layer antenna, also called a single-layer antenna, consists of a substrate layer on which the radiating element rests. Examples of such antennas are presented in [12]–[15]. Amendola *et al.* [12] and Milici *et al.* [15] demonstrated how epidermal antennas can be significantly sensitive to their environment. On the other hand, multi-layer antennas consist of at least two layers, a radiating element and a ground plane. Multi-layer antennas might include an EBG layer or yet multiple radiating elements with each radiator resting on a separate individual layer. Examples of this class of antennas, rather a more common category, can be seen in [16]–[18].

Generally, single-layer antennas are avoided in communication systems. This is because of significant radiation efficiency loss given the lack of a reflecting ground layer. Added to this is the extremely small spacing between the radiating element and body [19]. Multi-layer antennas, on the other hand, provide immunity to environment variations given the multiple protective layers found in its composition. The close proximity of the antenna to the skin may hinder skin respiration. Therefore, a single-layer antenna is preferred since it

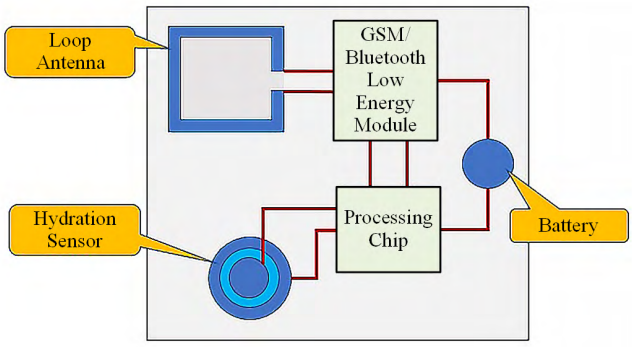

FIGURE 1. Concept art of a sensing epidermal device.

can be easily made porous to allow the cutaneous activity. A conceptual block diagram of the proposed biotelemetry device is shown in Fig. 1. The primary sensing components include body-hydration, glucose, and blood pressure sensors. This figure gives the intuition that for reliable sensing, it is necessary that the sensor must be placed extremely close to skin surface. Therefore, the sensor must be very thin and flexible in order to be comfortable for the user. Moreover, for short range communication, such as in the range of 1-5 meters, performance metrics such as antenna gain and radiation efficiency can be conceded. Thus, by considering the pros and cons of both BWA topologies, a single layer epidermal antenna was found to be more favorable and practical for our application as it provides comfortable and direct antenna placement on skin surface without any ground plane.

While selecting the antenna type, a one wavelength long loop antenna was compared to a small (magnetic) loop antenna. One wavelength long loop antenna was found to have superior performance based on the following facts. First of all, maximum power can be delivered to an antenna if it is in the order of a wavelength. Additionally, the reflection coefficient of the long loop antenna was experimentally determined to have better performance. On the other hand, small loop antennas have intrinsically higher complex input impedance and low radiation efficiency which further discourages its usage. Whereas, a one-wavelength long loop emulates an array consisting of two quarter-wave dipoles. This can be seen from the theoretical current distribution for a one wavelength long loop antenna shown in Fig. 2 (a).

In [20], we demonstrated how the performance of a square loop can be enhanced by adding four circular patches to it. The modified design is known as Quadruple Loop (QL) antenna. The enhancement can be appreciated by the fact that the simple square loop antenna provides 2% radiation efficiency and -12 dBi gain, whereas, the QL antenna provides 5% radiation efficiency and -10 dBi gain. This improvement was achieved by adding four circular patches to the main radiating side of the one-wavelength loop antenna. Moreover, this modification made the loop antenna better withstand frequency detuning when placed on different location on the arm. Table 1 lists the dimensions for the GSM-900,

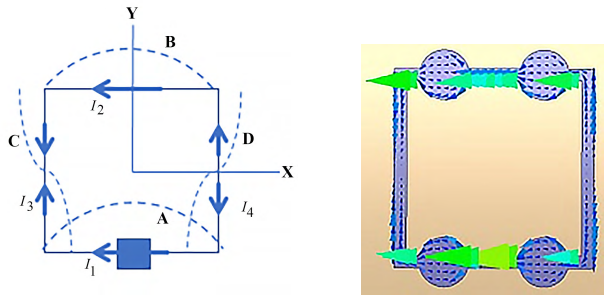

(a) (b)

FIGURE 2. Current distribution on (a) large loop antenna (b) QL BLE antenna at 2.4 GHz.

TABLE 1. Dimensions of the three QL antennas.

Antenna Application	Length (mm)	Width (mm)
GSM-900	32	32
GSM-1800	20	20
BLE	15	15

GSM-1800, and BLE QL antennas, whereas, Fig. 2 (b) shows the current distribution for the QL.

III. MODELING AND SIMULATIONS

Full-wave antenna simulations were performed with a biological tissue model. A stack of four layers (bone, muscle, fat, and skin) was used in the model to study antenna performance and wave propagation on a generic model of the human arm. It is important to note that, as the number of layers increase, the complexity burdens the simulator and its processing resources. The data values of the model were derived from [21].

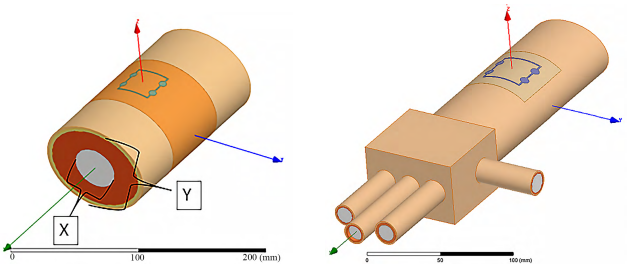

(a) (b)

FIGURE 3. (a) The cylindrical arm model and (b) the same model with a hand extension.

A. THE FOUR-LAYER MODEL

The arm was modeled as four concentric elliptical cylinders, each representing a body tissue. The inner most tissue is the bone, following that is the muscle layer which is covered by a thin fat layer and finally the skin, which acts as the most outer layer. The model is shown in Fig. 3 (a). Fig. 3 (b) shows the same model with the addition of a hand extension. The

TABLE 2. Dielectric parameters of arm tissues [21].

Tissue	Frequency (GHz)	Relative Permittivity	Loss Tangent
Skin	0.9	41.40	0.42
	1.8	38.87	0.30
	2.45	38.00	0.28
Fat	0.9	5.46	0.19
	1.8	5.349	0.15
	2.45	5.280	0.15
Muscle	0.9	55.03	0.34
	1.8	53.55	0.25
	2.45	52.73	0.24
Bone	0.9	12.45	0.23
	1.8	11.78	0.23
	2.45	11.38	0.25

TABLE 3. Dimensions of the cylindrical model.

Tissue	X (mm)	Y (mm)
Skin	64	45
Fat	60	42
Muscle	54	38
Bone	30	24

dielectric parameters for each layer are presented in Table 2, while the dimensions for major and minor axes for each cylinder are presented in Table 3.

B. THE SINGLE-LAYER EQUIVALENT MODEL

As each of the four tissues comprising the HFSS arm model has its own frequency dependent values of relative permittivity and loss tangent, it was important to find an equivalent model comprised of just a single lossy dielectric with its own frequency-dependent parameters to reduce simulation time. The original four-layer model was translated into a single-layer arm model by solving a 4 parallel-plate capacitor (PPC) system. This helped in determining the frequency dependent effective relative permittivity of the four layers of the body which was used in an HFSS unipolar Debye model to come up with an equivalent single-layer arm model.

The currents induced by the antenna travels back and forth along the arm which can be modeled as four parallel plate capacitors with length of the arm and separation gaps of body layers thicknesses. The plates are hollow ellipses surfaces and their respective bio-dielectrics are hollow elliptical cylinders.

The capacitance at any frequency for each tissue is computed by:

$$C_{Tissue} = \frac{\epsilon_0 \epsilon_r(f) A}{d}, \tag{1}$$

where, $\epsilon_r(f)$ is the frequency-dependent relative permittivity for a given tissue; this could be obtained from [21]. Given the parallel capacitance configuration of the fours tissues,

the total equivalent capacitance is

$$C_{eq} = C_{Skin} + C_{Fat} + C_{Muscle} + C_{Bone}, \tag{2}$$

whereas, the equivalent relative permittivity is computed as

$$\epsilon_{eq}(f) = \frac{C_{eq}}{C_0}. \tag{3}$$

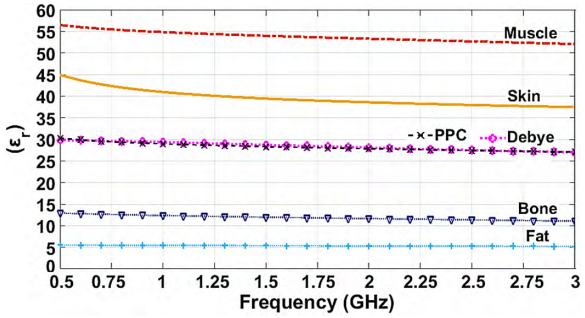

FIGURE 4. Relative permittivity vs. frequency for different tissues and models.

These equations were used to numerically determine $\epsilon_{eq}(f)$ from 0.5 GHz to 3 GHz. The equivalent relative permitivity found using PPC model is shown in Fig. 4 along with other tissues.

Based on the relative permittivity values obtained using the PPC computations for the upper and lower frequencies of 0.5 GHz and 3 GHz, relative permittivity values were approximated ($30.26 \rightarrow 30$ at 0.5 GHz and $27.04 \rightarrow 27$ at 3 GHz) and then assigned to the unipolar Debye model tool in HFSS to determine loss tangent, which was calculated to be 0.4 at 0.5GHz and 0.25 at 3 GHz. The resulting Debye model used in HFSS is given as

$$\epsilon_{eq}(f) = 24.63 + \frac{5.37}{1 + 1.41 \times 10^{-19} \times f^2}. \tag{4}$$

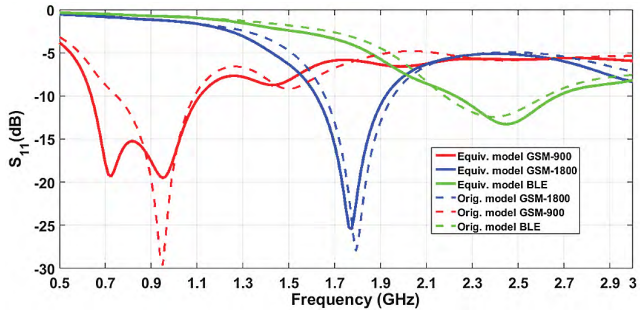

FIGURE 5. Comparison of reflection coefficient values for the original and equivalent HFSS models.

Fig. 4 demonstrates the relative permittivities of muscle, skin, bone, and fat versus frequency. In addition, the two modeling methods used, namely, the Debye model equivalent and the parallel plate capacitor (PPC) equivalent. The comparison of the reflection coefficients for the three QL antennas, when placed on the original four-layer model with its one-layer equivalent, is presented in Fig. 5.

TABLE 4. Wavelengths and penetration depths for tissues at different frequencies [21].

Frequency	Material	Wavelength (mm)	Penetration depth (mm)
900 MHz	Skin	50.71	40.23
	Fat	141.92	244.12
	Muscle	44.28	42.36
	Bone	93.78	131.57
	Air	333.10	—
1.8 GHz	Skin	26.42	28.25
	Fat	71.82	157.05
	Muscle	22.59	29.19
	Bone	48.20	66.65
	Air	166.55	—
2.45 GHz	Skin	19.66	22.57
	Fat	53.11	117.02
	Muscle	16.73	22.33
	Bone	35.99	45.78
	Air	122.36	—

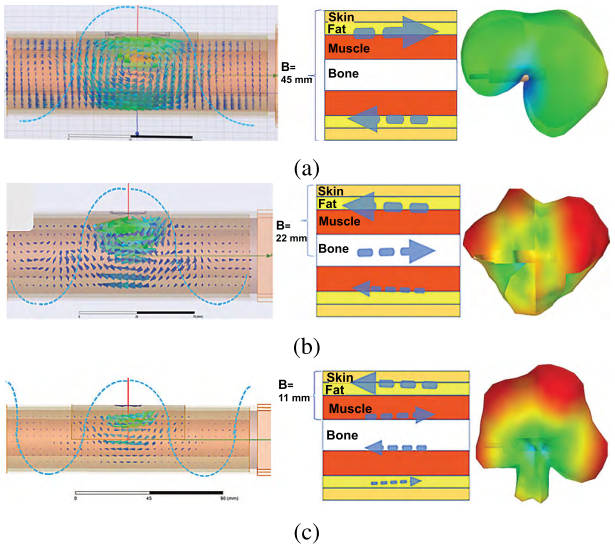

FIGURE 6. From the left to right: current distributions, simplified current distributions, and 3D radiation patterns at (a) 900 MHz , (b) 1.8 GHz, and (c) BLE (2.4 GHz).

C. SIMULATED CURRENT DISTRIBUTION AND RADIATION PATTERNS

In this section, we will discuss the current distribution within the equivalent cylindrical arm model as well as the 3D radiation pattern of the antennas at their corresponding frequency bands. Penetration depths as well as the electrical lengths of the arm layers will all be used to find an explanation for the shape of the radiation pattern at the three different frequencies, Table 4. A stack of tissue layers depicting the broadside view of the arm model can be seen in the middle of Fig. 6 for all the three frequencies. The current distribution within the tissue is approximated and portrayed in the stacked model. While "B" dimension corresponds to the start and end points of half-wavelength current distributions across the vertical dimension (height of the arm).

The antennas were designed to be one wavelength long at their respective operational frequencies. The wavelengths at 900 MHz, 1.8 GHz and 2.5 GHz can be observed across the horizontal dimension of the arm in the left column of Fig. 6 (a), (b) and (c), respectively. As can be seen in Fig. 6 (a), the length of B corresponds to approximately that of, height of the arm (vertical dimension). Given these values at 900 MHz and the actual thicknesses of the layers, it would be intuitive to say that a normally incident EM (electromagnetic) wave at 900 MHz on the top layer of the model, will make it through the whole stack and exit, retaining more than 37% of its power. Hence, significant through-arm radiation can be observed in the 3D radiation pattern.

At 1.8 GHz, the total length of the arm (horizontal dimension) is slightly greater than 1.5 times the electrical length of the antenna. Therefore, across the vertical dimension, current that reaches the vertical side of the arm, still makes some through arm radiation since the penetration depths are still large enough allowing EM waves to pass through with around 37% of its original power, Fig. 6 (b). It can also be observed that ''B'' is approximately half the height of the arm (vertical dimension) at this frequency. Compared to the radiation pattern at 900 MHz, the pattern at 1.8 GHz is more directive as depicted from the red colored peak of the radiation pattern in the right most column of Fig. 6 (b).

The physical length of each side of the BLE antenna corresponds to one-quarter wavelength of operation at 2.45 GHz. As a result of shorter wavelengths at this frequency the penetration depths are less and it can be seen in Fig. 6 that the currents induce within tissues attenuate much faster compared to 900 MHz and 1800 MHz. Hence, through-arm radiation is very low and is only visible right below the antenna location. Compared to the patterns at 900 MHz and 1.8 GHZ, the pattern at 2.45 GHz is the most directive, right column of Fig. 6. It can be inferred from our results that, at higher frequency, the radiation pattern of an epidermal antenna resembles that of a simple patch antenna.

IV. FABRICATION AND MEASUREMENTS

A. FABRICATION

Different types of flexible and stretchable materials can be used to realize the body-worn antenna. The use of flexible materials would be of significant value for epidermal antennas applications because the antenna structure is desired to be conformable to the skin surface. A prime example is polymer-based materials, such as Dupont's Kapton polyimide, the silicon-based elastomer poly-dimethylsyloxane (PDMS), and the FDA-approved skin adhesive Tegaderm. The major advantage of using polymers lies in their flexibility and strength which all arise from the strong intermolecular forces present in their structure.

The epidermal QL antennas presented here were fabricated using 75 microns thick Kapton substrates. For conductive layer, adhesive copper sheets were used. Photographs of the fabricated antennas are shown in Fig. 7.

(a) (b) (c)

FIGURE 7. The fabricated QL antennas, (a) GSM-900 and (b) GSM-1800 (C) BLE.

The radiating elements were cut into shape by an LPKF milling machine.

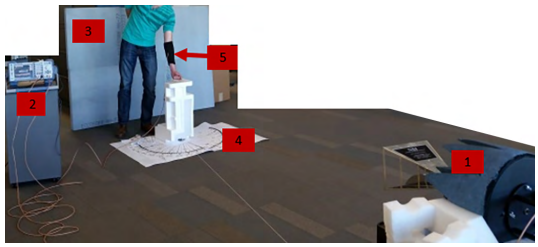

FIGURE 8. The setup for radiation pattern measurements.

B. MEASUREMENTS

Measuring the performance of any epidermal antenna is an arduous job since it requires a human volunteer as a part of the test bench. However, the determination of the radiation patter is important to understand the actual performance of the antenna. Usually, physical body phantoms are used for body-worn antenna performance evaluation and radiation pattern measurements. This is due to the inconvenience of prolonged stationary posture necessary for reliable measurements. In addition, the access to large enough anechoic chambers that could house a volunteer is uncommon. Therefore, we took the measurements using a human volunteer in an open environment. The measurement setup, shown in Fig. 8, includes

1) a wide-band ridged horn antenna, NSI-RF-RGP-10, to act as a probe,
2) a R&S®ZVL13 Vector Network Analyzer,
3) some Microwave absorbers (Eccosorb AN-77) ,
4) a 1-meter diameter paper protractor,
5) a compression band to keep the epidermal antenna fixed in place,
6) a (20×12) m^2 room.

To place the Kapton-printed antenna on the arm, a compression band was used during the experimentation. The antenna was positioned in a manner which oriented the feed port of the antenna identical to that of the simulations performed. The epidermal antenna under the test was connected to one port of the VNA while the horn antenna was connected to the other port. Whereas, measurements were taken by

keeping the arm at the center of a protractor, which was used to measure the angle of rotation.

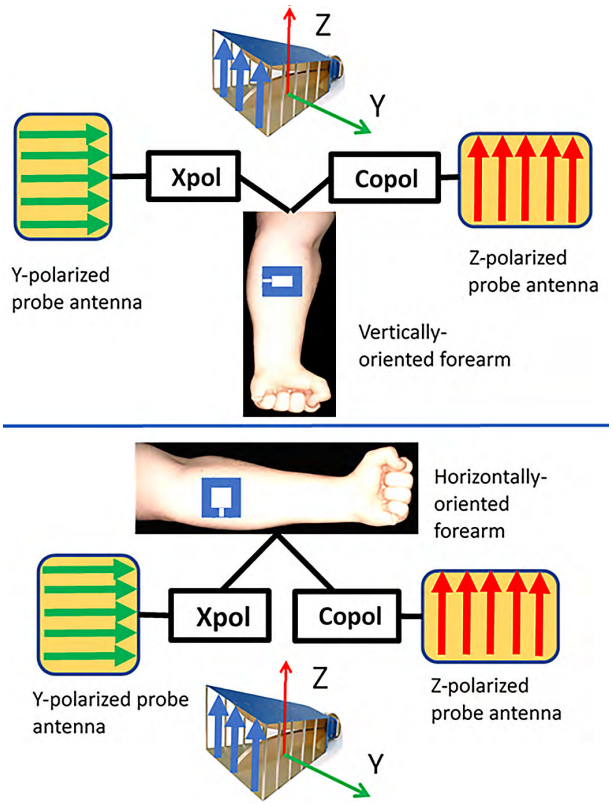

FIGURE 9. Configurations of radiation pattern measurements.

The measurements covered four different arm and probe antenna orientations as seen in Fig. 9. Each arm orientation (vertical and horizontal) was used to measure cross-polarization (Xpol) and co-polarization (Copol) pattern. To achieve this, the probe antenna was oriented in two different orientations, Fig. 9. The arm would be oriented either perpendicular (vertical arm) or parallel (horizontal arm) to the floor. In turn, the probe antenna would measure 120 degrees of the radiation pattern. This was done twice to cover the Z(Copol) and Y(Xpol) probe-antenna orientations. The similar steps were used for all the three QL antennas.

According to [9], when attached to a human body, most antennas exhibit a radiation pattern similar to that of a patch antenna. This behavior was also observed during the course of our antenna testing at frequencies around and above 1 GHz. It was observed in the experiments that a small separation (about 1-3 mm) between body and antenna is sufficient to keep the user's body from the reactive near-field of the antenna. This is important to note as the reactive near-field determines the input impedance of a closely spaced wearable antenna, hence, affecting its bandwidth, gain and efficiency.

1) GSM-900 ANTENNA

Fig. 10 shows the measured and simulated reflection coefficient of the designed antenna. The discrepancy in the

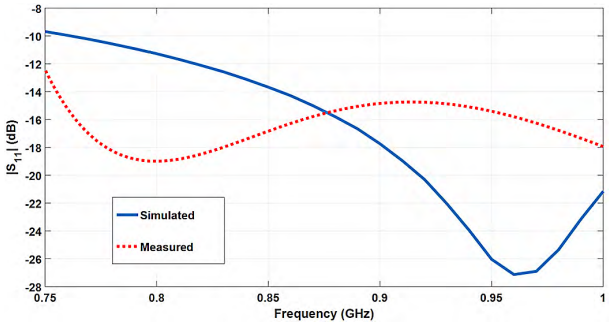

FIGURE 10. Measured and simulated reflection coefficient for the GSM-900 QL antenna.

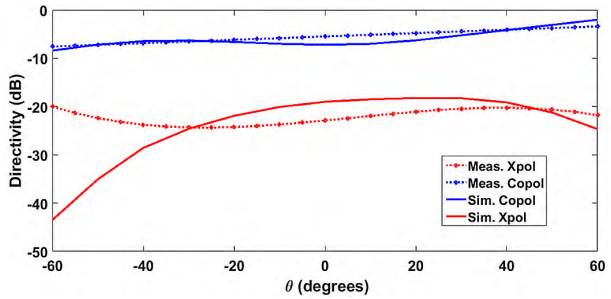

FIGURE 11. Radiation patterns for the vertical arm at 900 MHz.

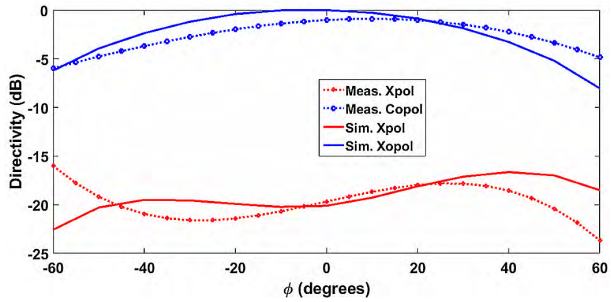

FIGURE 12. Radiation patterns for the horizontal arm at 900 MHz.

measured results can be attributed to the variation of the body parameters and fabrication inaccuracies incurred during the use of milling and cutting the adhesive flexible copper sheets. Nevertheless, the antennas shows good reflection coefficient in the desired bandwidth.

The radiation patterns of the antenna are shown in Fig. 11 12. The patterns obtained at this frequency reveal a good match between simulated and measured results. At 900 MHz, the wavelength is longer compared to the arm, allowing the waves an easy pass-thorough and thus substantial radiations are received at the back side. In fact, the arm becomes invisible to the waves and allows signal reception from all the directions thus improving the mobility.

2) GSM-1800 ANTENNA

The measured and simulated reflection coefficient of the antenna designed at 1.8 GHz is shown in Fig. 13. Similar to

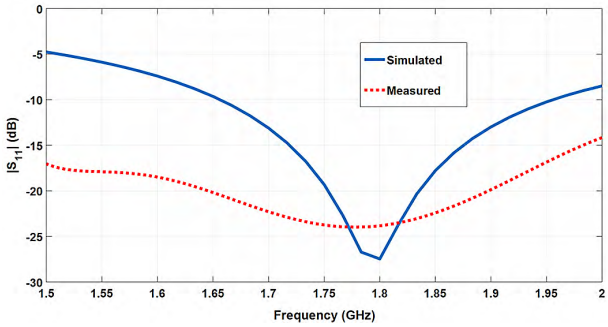

FIGURE 13. Measured and simulated reflection coefficient for the GSM-1800 QL antenna.

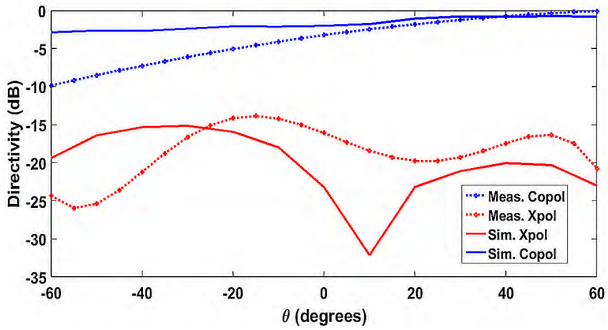

FIGURE 14. Radiation patterns for the vertical arm at 1.8 GHz.

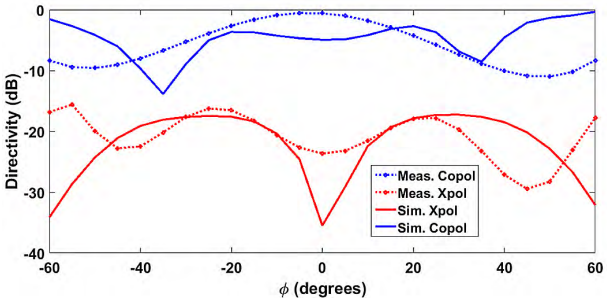

FIGURE 15. Radiation patterns for the horizontal arm at 1.8 GHz.

the 900 MHz, EM waves at 1.8 GHz are also less affected by the presence of the arm due to diffraction properties of the longer wave. Since GSM-1800 antennas are usually intended for cellular applications, transmission and reception are desired to be omni-directional. These features were realized to a certain degree in the radiation patterns seen in Fig. 14 and Fig. 15.

3) BLE ANTENNA

For the results of BLE 2.4 GHz antenna, a good agreement between the measured and simulated reflection coefficient was observed. The results are shown in Fig. 16. The lower reflection coefficient values in the measured results that the simulated can be attributed to higher losses in the actual scenario.

As can be inferred from Fig. 17, there is a difference of more than 15 dB between the peaks of the co- and cross-polarizations for the vertical orientation of the arm. The

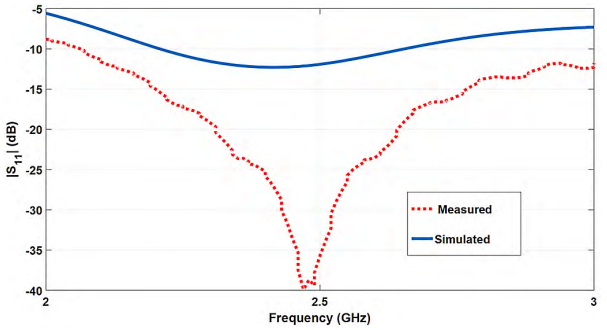

FIGURE 16. Measured and simulated reflection coefficient for the QL BLE antenna.

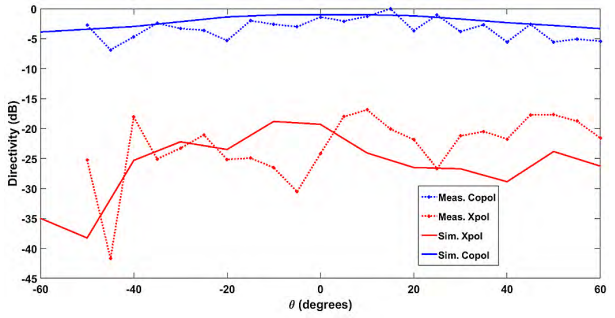

FIGURE 17. Radiation patterns for the vertical arm at 2.4 GHz.

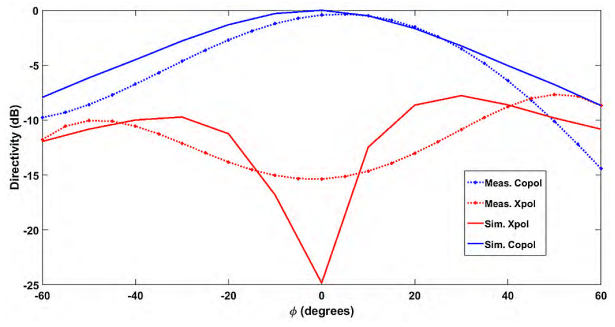

FIGURE 18. Radiation patterns for the horizontal arm at 2.4 GHz.

Copol looks almost completely uniform when compared to the bumpy pattern of its Xpol counterpart. For simulation patterns of the horizontal arm, Fig. 18, a difference of 25 dB between the relatively symmetric maximum of the Copol and minima of the Xpol can be seen.

For robust interpretation, all the presented measurement results were obtained by averaging the data. To appreciate the degree of variation, we have shown the raw measurement curves for both of the cross-polarization and co-polarization at 2.4 GHz in Fig. 17. These were measured for the vertical positioned arm. The results illustrate good agreement between the simulated and measured radiation pattern.

It should be noted that the fabricated copper antennas, especially those which were made with the LPKF machine, were not an exact replica of the original software designs.

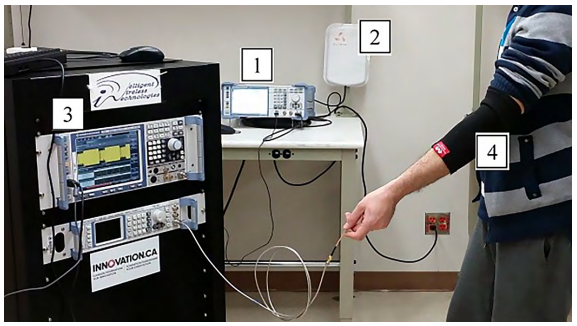

FIGURE 19. Data communication measurement setup.

This is due to fabrication inaccuracies incurred through the use of drilling needles and cutting through adhesive flexible copper sheets. As mentioned before, these minute differences have a more pronounced effect on measurement results at higher frequencies. Nonetheless, the level of similarity between simulated and measured results were unexpected given the priori of the unpredictability of single-layer body-worn antennas. The matching level between the majority of the simulated and measured radiation patterns was good. As previously noted, the differences lie mostly in the relative locations of the troughs and crests of the patterns.

V. DATA COMMUNICATION TESTS

A true measure of antenna efficiency would be to test its performance in a real wireless communications link. Hence, the GSM-900 and the BLE/ISM (2.4-2.5) GHz antennas were each tested for their error vector magnitudes (EVM) in a real-time link. EVM is a measure of how accurately a radio device is transmitting or receiving symbols within a constellation. The root-mean-square of the EVM for all received symbols is calculated as in [22],

$$EVM_{RMS}(\%) = \sqrt{\frac{P_{error}}{P_{reference}}} \times 100\%, \tag{5}$$

where, P_{error} is the power (magnitude) of the error vector and $P_{reference}$ is the power of the reference ideal point. The vector signal generator (VSG) was set-up to generate 4-QAM packets at a frequency of 915 MHz for the epidermal GSM-900 antenna and then at 2.45 GHz for the epidermal BLE antenna. The Epidermal antennas were worn as receiving antennas and were connected to an R&S FSV, signal analyzer. Fig. 19 shows the measurement setup that includes

1) R&S®SMBV100A Vector Signal Generator: this device acted as the transmit system where the frequency, modulation and power levels were set,
2) transmit antennas:
   a) RP circular 915 MHz antenna (ALR-9611-CR),
   b) Omni-directional 2.45 GHz antenna (CAF94150 030421),
3) R&S®FSV Signal and Spectrum Analyzer: this device provided real time measurements of EVM as well as real time display of the constellation diagrams,

FIGURE 20. Arm-body orientation states with respect to the transmit antenna.

TABLE 5. Communication tests results with the respective TX/RX antenna orientations.

State	Frequency	P_T (dBm)	EVM_{RMS} (%)
1	915 MHz	-10	17.55
		0	9.23
		10	2.10
1	2.45 GHz	-10	8.10
		0	2.29
		10	0.75
2	915 MHz	-10	18.04
		0	13.70
		10	5.31
2	2.45 GHz	-10	6.10
		0	3.52
		10	1.33
3	915 MHz	-10	16.20
		0	14.00
		10	7.45
3	2.45 GHz	-10	16.05
		0	12.88
		10	3.75

4) Receive epidermal antennas:
   a) Kapton-based adhesive copper GSM-900 antennas,
   b) Kapton-based adhesive copper BLE antennas.

Communication tests for both frequencies (915 MHz and 2.45 GHz) involved various arm-body orientation and position states, as shown in Fig. 20. In addition, the measurements were performed using different transmit power levels of −10 dBm, 0 dBm, and 10 dBm. A power level of 10 dBm is relatively high for body-worn applications and it was used only for research and experimentation purposes. Results for these tests are presented in Table 5.

Although EVM_{RMS} results provide adequate information about the performance of the receiver system, bit-error-rate (BER) is a more popular means to gauge the performance of a communications system, and this is particularly true with GSM standards. Hence, in order toconvert EVM_{RMS} values into corresponding BER, we used the equation as in [23],

$$BER = Q\left(\frac{1}{EVM_{RMS}}\right), \tag{6}$$

where $Q(\cdot)$ is the Gaussian co-error function, calculated as as,

$$Q(x) = \int_x^{\infty} \frac{1}{\sqrt{2\pi}} \left(e^{-\frac{y^2}{2}}\right) dy. \tag{7}$$

Fig. 21 shows BER versus EVM for a 4-QAM standard.

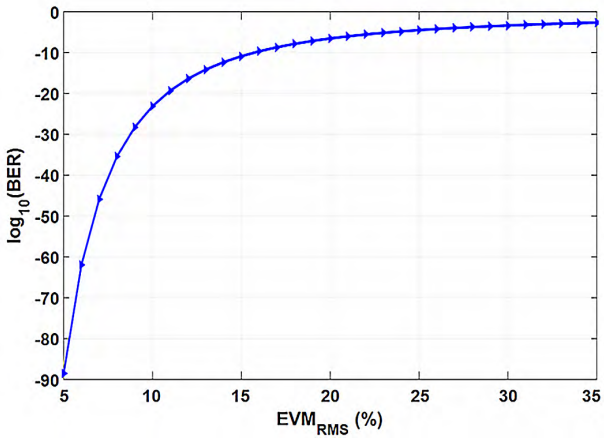

FIGURE 21. BER versus EVM for a 4-QAM.

Since all the measured EVM values are better than 19%, their translation into corresponding BER values yield less than 0.1% (1 erroneous bit in a 1000 bits). For the Bluetooth communications, a minimum receiver sensitivity of −70 dBm with a BER of 0.1% or better is required. According to the plot in Fig. 21, 0.1% percent corresponds to an EVM value of about 30%. Although the calculated received powers shown below are not less than −52.7 dBm, it is expected that even at −70 dBm the BER would not exceed 0.1%. This can be inferred from when the transmitted power was decreased from 0 to −10 dB, the EVM values for both BLE and GSM-900 antennas increased to no more than 4-5%. Hence, it is expected that if the received power was at −70 dBm we should expect EVM values of no more than 25% which correspond to BER values of better than 0.1%.

VI. CONCLUSION

The human body surely poses significant challenges when used as an antenna platform. As analysis tools, different HFSS arm models composed of skin, fat, muscle and bone layers were used throughout the project. The four-layer cylindrical model was later adopted as the standard model to help explain the shape of the radiation pattern for the designed epidermal antennas. From then, it was desired to find an equivalent arm model consisting of only one lossy dielectric instead of the four tissue-representing layers. This serves as a more efficient means for resource allocation and simulation runtime. In addition, this equivalent model can be realized into a physical phantom whose dielectric parameters could be recreated by chemical recipes. Furthermore, QL epidermal antennas were designed and tested for GSM-900, GSM-1800 and BLE. They were fabricated using very thin, single-layer groundless structures to allow for the accommodation of neighboring electronics and sensors. Radiation patterns and reflection coefficient were measured that show good agreement with simulated results. Finally, data communication tests depicted that the acquired BER could qualify this antenna technology to work in a 4- QAM wireless link.

REFERENCES

[1] H. A. Damis, "Epidermal loop antennas," M.S. thesis, Dept. Elect. Comput. Eng., Univ. Alberta, Edmonton, AB, Canada, 2017.
[2] M. M. Hassan, H. Albakr, H. Al-Dossari, and A. Mohamed, "Resource provisioning for cloud-assisted body area network in a smart home environment," *IEEE Access*, vol. 5, pp. 13213–13224, 2017.
[3] E. Cianca, M. De Sanctis, and S. Di Domenico, "Radios as sensors," *IEEE Internet Things J.*, vol. 4, no. 2, pp. 363–373, Apr. 2017.
[4] Q. Huang, W. Wang, and Q. Zhang, "Your glasses know your diet: Dietary monitoring using electromyography sensors," *IEEE Internet Things J.*, vol. 4, no. 3, pp. 705–712, Jun. 2017.
[5] M. Grimm and D. Manteuffel, "Body worn antenna system for health care related on- and off-body communications," in *Proc. EAI 4th Int. Conf. Wireless Mobile Commun. Healthcare (Mobihealth)*, Nov. 2014, pp. 203–206.
[6] S. Amendola and G. Marrocco, "Optimal performance of epidermal antennas for uhf radio frequency identification and sensing," *IEEE Trans. Antennas Propag.*, vol. 65, no. 2, pp. 473–481, Feb. 2017.
[7] X. Huang *et al.*, "Epidermal radio frequency electronics for wireless power transfer," *Microsyst. Nanoeng.*, vol. 2, Oct. 2016, Art. no. 16052.
[8] MICS. (2017). *47 CFR I—Medical Implant Communications (MICS)*. [Online]. Available: https://www.gpo.gov
[9] T. Kellomaki, J. Heikkinen, and M. Kivikoski, "One-layer GPS antennas perform well near a human body," in *Proc. 2nd Eur. Conf. Antennas Propag. (EuCAP)*, Nov. 2007, pp. 1–6.
[10] S. Zhang, A. Paraskevopoulos, C. Luxey, J. Pinto, and W. Whittow, "Broad-band embroidered spiral antenna for off-body communications," *IET Microw., Antennas Propag.*, vol. 10, no. 13, pp. 1395–1401, 2016.
[11] Z. H. Jiang, M. D. Gregory, and D. H. Werner, "Design and experimental investigation of a compact circularly polarized integrated filtering antenna for wearable biotelemetric devices," *IEEE Trans. Biomed. Circuits Syst.*, vol. 10, no. 2, pp. 328–338, Apr. 2016.
[12] S. Amendola, S. Milici, and G. Marrocco, "Performance of epidermal RFID dual-loop tag and on-skin retuning," *IEEE Trans. Antennas Propag.*, vol. 63, no. 8, pp. 3672–3680, Aug. 2015.
[13] H. R. Khaleel, "Design and fabrication of compact inkjet printed antennas for integration within flexible and wearable electronics," *IEEE Trans. Compon., Packag., Manuf. Technol.*, vol. 4, no. 10, pp. 1722–1728, Oct. 2014.
[14] G. Marrocco, "RFID antennas for the UHF remote monitoring of human subjects," *IEEE Trans. Antennas Propag.*, vol. 55, no. 6, pp. 1862–1870, Jun. 2007.
[15] S. Milici, S. Amendola, A. Bianco, and G. Marrocco, "Epidermal RFID passive sensor for body temperature measurements," in *Proc. IEEE RFID Technol. Appl. Conf. (RFID-TA)*, Sep. 2014, pp. 140–144.
[16] S. Zhu and R. Langley, "Dual-band wearable textile antenna on an EBG substrate," *IEEE Trans. Antennas Propag.*, vol. 57, no. 4, pp. 926–935, Apr. 2009.
[17] S. Kim, Y.-J. Ren, H. Lee, A. Rida, S. Nikolaou, and M. M. Tentzeris, "Monopole antenna with inkjet-printed EBG array on paper substrate for wearable applications," *IEEE Antennas Wireless Propag. Lett.*, vol. 11, pp. 663–666, 2012.
[18] M. A. B. Abbasi, S. S. Nikolaou, M. A. Antoniades, M. N. Stevanović, and P. Vryonides, "Compact EBG-backed planar monopole for BAN wearable applications," *IEEE Trans. Antennas Propag.*, vol. 65, no. 2, pp. 453–463, Feb. 2017.
[19] D. Werner and Z. Jiang, *Electromagnetics of Body Area Networks: Antennas, Propagation, and RF Systems*. Hoboken, NJ, USA: Wiley, 2016.
[20] H. A. Damis, R. Mirzavand, H. J. Chung, and P. Mousavi, "Flexible printed square loop antennas for wearable applications," in *Proc. 17th Int. Symp. Antenna Technol. Appl. Electromagn. (ANTEM)*, Jul. 2016, pp. 1–2.
[21] R. F. D. Andreuccetti and C. Petrucci. (1997). *An Internet Resource for the Calculation of the Dielectric Properties of Body Tissues in the Frequency Range 10 Hz–100 GHz*. [Online]. Available: http://niremf.ifac.cnr.it/tissprop/
[22] R. A. Shafik, M. S. Rahman, and A. R. Islam, "On the extended relationships among EVM, BER and SNR as performance metrics," in *Proc. Int. Conf. Elect. Comput. Eng.*, Dec. 2006, pp. 408–411.
[23] R. Zhang, J. Ma, and X. Xin, "Full-duplex fiber-wireless link for alternative wired and 40-GHz band wireless access based on differential quaternary phase-shift optical single sideband millimeter-wave signal," *Opt. Eng.*, vol. 54, no. 2, p. 026101, 2015.

HAITHAM ABU DAMIS (S'14) graduated from the Canadian University of Dubai (CUD) in 2014 with a BSc. degree in Telecommunications Engineering. Throughout his BSc. years, he worked extensively with Wireless Sensor Networks (WSNs). During his internship term at the University of Quebec in Trois Rivieres (UQTR) he was involved with FPGA prototyping and programming. In September 2014, he joined Dr. Mousavi's group as an MSc. student at the University of Alberta. During that time and until his graduation in 2017, he worked extensively with flexible electronics and body-worn antennas.

NABIL KHALID (S'15) received the bachelor's degree in electrical engineering from Air University, Islamabad, Pakistan, in 2013, and the M.Sc. degree in electrical and computer engineering from Koç University, Istanbul, Turkey, in 2017, with a focus on developing the physical layer of THz Band wireless communications. He is currently pursuing the Ph.D. degree with the Electrical and Computer Engineering Department, University of Alberta, Edmonton, Canada, under the supervision of Prof. P. Mousav, with a focus on designing efficient MIMO antennas. His majors involved in telecommunications, RF/microwave, and RADARs. Following his undergrad he was with the RF/Microwave Department, RWR Pvt. Ltd., Islamabad, Pakistan, from 2013 to 2014, as a Design Engineer, with a focus on designing industrial grade power amplifiers. From 2015 to 2017, he was with the Next-Generation and Wireless Communications Laboratory, as a Research Assistant. In 2017, he joined the Intelligent Wireless Technologies Laboratory as a Research Assistant.

RASHID MIRZAVAND (M'12–SM'16) received the B.Sc. degree from the Isfahan University of Technology, Isfahan, Iran, in 2004, and the M.Sc. and Ph.D. degrees from the Amirkabir University of Technology (Tehran Polytechnic), Tehran, Iran, in 2007 and 2011, respectively, all in electrical engineering.

Since 2011, he has been a Research Professor with the Amirkabir University of Technology. He is currently a Research Associate with the Intelligent Wireless Technology Laboratory, University of Alberta, Edmonton, AB, Canada. He has authored over 85 papers published in refereed journals and conferences proceedings. His research interests include integrated sensors and microwave/millimeter-wave circuits.

Dr. Mirzavand was a recipient of the Best Ph.D. Thesis Award from the Amirkabir University of Technology in 2012, the Best National ICT Researcher Award from the Ministry of Information and Communications Technology of Iran in 2013, the Elite Young Researcher Grant Award from Iran's NEF in 2014, and the Alberta Innovates Technology Futures Elite Postdoctoral Fellowship Award in 2015.

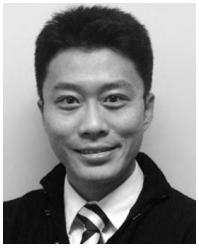

HYUN-JOONG CHUNG received the B.S. degree from the Korea Advanced Institute of Science and Technology in 2000 and the Ph.D. degree from the University of Pennsylvania in 2005. His thesis is about phase separation and wetting/dewetting of polymer blend coatings and on the effect of nanoparticles. He was with Samsung Mobile Display, South Korea, as a Senior Engineer. He contributed to developing prototype large-area OLED TVs, while he developed expertise in thin film transistors from ZnO-based oxide semiconductors. From 2009 to 2012, he performed research on skin-like biochemical sensors and silicon electronics for bio-integrated devices with the University of Illinois at Urbana–Champaign. Since 2013, he has been a Faculty Member with the University of Alberta.

PEDRAM MOUSAVI (M'00–SM'14) received the B.Sc. (Hons.) degree in Telecommunication Engineering from Iran University of Science and Technology, Tehran, in 1995 and the M.Sc. and Ph.D. degrees from the University of Manitoba, Winnipeg, Canada, in 1997 and 2001 respectively, all in Electrical Engineering.

He is a Professor with Departments of Mechanical Engineering and NSERC-AITF Industrial Research Chair in Intelligent Integrated Sensors and Antennas at the University of Alberta. Dr. Pedram Mousavi has over fifteen years of entrepreneurial academic experience with start-up companies from the University of Waterloo and the University of Alberta. He founded Intelwaves Technologies as a spin-off from the University of Waterloo. He is a co-founder of WiDyne Technologies to commercialize the single-conductor technology from the University of Alberta.

His current mission is to foster a strong collaboration between industry and academia and stimulate more industry relevant research in wireless technologies. The research conducted through this industrial chair program will allow ICT (information and communications technology) innovations to be applied to the areas of intelligent integrated sensors and antennas to improve the productivity of the oil-energy sector and to sustain its growth. Dr. Mousavi has more than 150 refereed journal and conference articles and several patents in this field. His research interests are in the areas of advanced intelligent antenna, microwave and millimetre-waves circuits and systems, 5G phased array antennas, UWB radar systems, 3-D printing electronics and single conductor power and data transmission.